CD8^{+} Tumor-Infiltrating T Cells Are Trapped in the Tumor-Dendritic Cell Network[1,2]

Alexandre Boissonnas[*,†,‡], Fabrice Licata[*,†,‡], Lucie Poupel[*,†,‡], Sébastien Jacquelin[*,†,‡], Luc Fetler[§], Sophie Krumeich[¶], Clotilde Théry[¶], Sébastian Amigorena[¶] and Christophe Combadière[*,†,‡]

*Institut National de la Santé et de la Recherche Médicale, UMR S945, Immunité et Infection, Hôpital Pitié-Salpêtrière, Paris, France; †Université Pierre et Marie Curie (UPMC), Université Paris 06, UMR S945-IUC, Paris, France; ‡Assistance Publique–Hôpitaux de Paris, Groupe Hospitalier Pitié-Salpétrière, Service d'Immunologie, Paris, France; §Centre National de la Recherche Scientifique, UMR 168, Laboratoire de Physico-Chimie Curie, Institut Curie, Paris, France; ¶Institut National de la Santé et de la Recherche Médicale, U932, Immunité et Cancer, Institut Curie, Paris, France

Abstract

Chemotherapy enhances the antitumor adaptive immune T cell response, but the immunosuppressive tumor environment often dominates, resulting in cancer relapse. Antigen-presenting cells such as tumor-associated macrophages (TAMs) and tumor dendritic cells (TuDCs) are the main protagonists of tumor-infiltrating lymphocyte (TIL) immunosuppression. TAMs have been widely investigated and are associated with poor prognosis, but the immunosuppressive activity of TuDCs is less well understood. We performed two-photon imaging of the tumor tissue to examine the spatiotemporal interactions between TILs and TuDCs after chemotherapy. In a strongly immunosuppressive murine tumor model, cyclophosphamide-mediated chemotherapy transiently enhanced the antitumor activity of adoptively transferred ovalbumin-specific CD8^{+} T cell receptor transgenic T cells (OTI) but barely affected TuDC compartment within the tumor. Time lapse imaging of living tumor tissue showed that TuDCs are organized as a mesh with dynamic interconnections. Once infiltrated into the tumor parenchyma, OTI T cells make antigen-specific and long-lasting contacts with TuDCs. Extensive analysis of TIL infiltration on histologic section revealed that after chemotherapy the majority of OTI T cells interact with TuDCs and that infiltration is restricted to TuDC-rich areas. We propose that the TuDC network exerts antigen-dependent unproductive retention that trap T cells and limit their antitumor effectiveness.

Neoplasia (2013) 15, 85–94

Introduction

Unexpected observations have been reported in cancer clinical trials and animal models following the combination of chemotherapy and immunotherapy [1]. Indeed, improved prognoses after cancer vaccine [2] or adoptive cell [3] therapies have been observed when immunotherapeutic agents are administered in combination with chemotherapeutic regimens. Conventional cancer therapies are primarily based on the preferential targeting of tumor cells, which are actively proliferating and require higher quantities of growth factors and nutrients than healthy tissues. It has been shown that direct cytotoxicity toward tumor cells induces immunogenic cross-presentation of dying tumor cells [4,5] or sensitizing tumor cells to cytotoxic T lymphocyte (CTL) activity, both in human tumor cell lines [6] and mouse models [7]. Cyclophosphamide (CP) is an alkylating agent often used in cancer chemotherapy and for prevention of graft-*versus*-host disease [8]. Several reports describe a hematopoietic cell–mediated antitumor effect after CP treatment. The mechanisms involved are not well understood, but there is no doubt that CTLs also contribute to this antitumor activity. Increased tumor-specific T lymphocyte proliferation has been associated with the lymphoablative properties of CP [9,10]. CP has also been described to selectively deplete or inhibit immunosuppressive populations, such as regulatory T cells [11–13] and myeloid-derived suppressor cells [14]. The balance between immunostimulatory effects of chemotherapy and the immunosuppressive tumor environment has a complex outcome on the orchestration of T cell antitumor activity. Indeed, increased antitumor activity is mostly transient and tumor control relapses when a *de novo* equilibrium is reached through immunoselection and/or immunosubversion of the newly activated CTLs [15]. Antigen-presenting cells and especially tumor-associated macrophages (TAMs) and tumor dendritic cells (TuDCs) have been widely involved in tumor progression and immunosubversion of CTLs [16–19]. TAMs and TuDCs share common markers and their phenotypic distinction is still a matter of debate. Despite increasing knowledge in the processes of T cell immunosubversion by TAMs, the spatiotemporal orchestration of tumor-infiltrating lymphocytes (TILs)/TuDCs cross talk in living tissue has been poorly investigated. Deciphering the mechanisms by which antigen-presenting cells rapidly limit CTL-mediated destruction represents a prerequisite to improve the efficacy of therapeutic regimens.

Here, we used an intravital imaging approach to study in a highly immunosuppressive tumor model in mice how the TuDC network affects tumor-specific T lymphocyte infiltration after CP treatment.

Materials and Methods

Ethics Statement

Animal experiments were approved by the local Institutional Animal Care and Use Committee: Centre d'Exploration Fonctionnelle, Pitié-Salpétrière.

Mice

C57BL/6 female mice (6 to 10 weeks) were obtained from Charles River (Les Oncins, France). C57BL/6 $Rag2^{-/-}$ TCR (Vα2, Vβ5) transgenic mice (OTI) were crossed to CD45.1 C57BL/6, Actb-ECFP/BL6, or Actb-DsRed/BL6 (Animalerie Centrale, Institut Curie) to obtain OTI CD45.1, OTI-CFP, and OTI-DsRed mice, respectively. CD11c-YFP transgenic mice (CD11c-YFP) [20] were bred in our Animal Facility (Centre d'Exploration Fonctionnelle, Pitié-Salpétrière).

Cells

The MCA101 (MCA) cell line [21] (kindly provided by L. Zitvogel, Institut Gustave-Roussy, Villejuif, France) was stably transfected with a plasmid encoding for soluble ovalbumin (OVA) or a control plasmid (Mock) to generate MCA-OVA and MCA cell lines, respectively [22]. MCA cell lines were cultured in Dulbecco's modified Eagle's medium and the EL4 cell line in RPMI (Gibco, Invitrogen, Cergy Pontoise, France), supplemented with antibiotics and 10% fetal calf serum.

CD8$^+$ OTI T cells (specific for OVA$_{257–264}$ peptide in a H2-K^b context) and polyclonal CD8$^+$ T cells were either obtained from lymph nodes of OTI $Rag2^{-/-}$ mice (herein called OTI T cells, with a purity between 94% and 98%) or after magnetic beads sorting of lymph node cells from non-RAG OTI transgenic mice or from Actb-DsRed/BL6 for polyclonal CD8$^+$ T cells, using the CD8$^+$ negative sorting kit from Miltenyi Biotec (Paris, France) according to the manufacturer's instructions (purity above 90%).

In Vivo *Tumor Growth and Treatments*

MCA-OVA cells (2×10^5) were injected subcutaneously in the flank of mice. Tumor size was measured twice a week using a caliper, $V = L \times l \times (L + l)/2$. Chemotherapy was performed 7 days after tumor inoculation by a single intraperitoneal injection of CP (Sigma-Aldrich, Saint-Quentin Fallavier, France) diluted in phosphate-buffered saline (PBS) at 100 mg/kg. Adoptive T cell transfer was performed at day 10 after tumor inoculation by intravenous (i.v.) injection of 5×10^6 freshly harvested OTI T cells. For MCA tumor imaging, MCA cells were injected in a contralateral manner with MCA-OVA. For the kidney tumor model, 2×10^5 EL4 cells were injected i.v. This injection route induces secondary localization of EL4 cells into the kidney and leads to paraplegia within 18 to 25 days. Mice were sacrificed at the first step of paraplegia, considered as the end point of survival. Kaplan-Meier survival was then performed according to these criteria. For intravital imaging, 5×10^6 freshly harvested polyclonal CD8$^+$ T cells were adoptively transferred 3 days after EL4 inoculation to induce antigen-specific expansion and infiltration into the tumor.

Flow Cytometry

Phenotypic characterization of all cell populations was performed using either a FACSCalibur or FACSCanto II (Becton Dickinson, Franklin Lakes, NJ) for acquisition. For analysis, FlowJo software (Tree Star Inc, Ashland, OR) was used. MCA-OVA tumor and draining lymph node (axillary) were harvested at indicated days. MCA-OVA tumors and draining lymph node were entirely mashed in PBS with 0.5% BSA and filtered using 70-μm cell strainer (BD Biosciences, San Jose, CA). Surface staining was performed by incubating 50 μl of cell suspension (1/10th of the total) with 1 μg/ml purified anti-CD16/32 (2.4G2; BD Biosciences) for 10 minutes at 4°C and for an additional 20 minutes with appropriate dilution of specific antibodies. The following panel of surface antibodies was used: anti-CD11b (clone M1/70), anti-Ly6C (clone AL-21), anti-Ly6G (clone 1A8), anti-CD45 (clone 30-F11), anti-CD11c (clone HL3), anti–I-Ab (clone AF6-120.1), anti-CD8 (clone 53-6.7), anti-CD69 (clone H1.2F3), anti-CD45.1 (clone A20), anti–interferon-γ (IFN-γ) (clone XMG1.2), anti-IL4Rα from Pharmingen, BD Biosciences, anti-F4/80 (clone BM8) from eBioscience (Paris, France), and anti-Mgl1 from AbD Serotec (Colmar, France). After incubation, cell suspensions were washed once in PBS with 0.5% BSA. For intracellular cytokine staining, cell suspensions were restimulated *ex vivo* with 1 μM OVA$_{257–264}$ for 3 hours at 37°C in the presence of 5 μg/ml Brefeldin A. After surface staining, cells were fixed in

4% paraformaldehyde (PFA) for 20 minutes, washed twice in perm/wash solution (BD Biosciences), and incubated for 20 minutes in perm/wash in the presence of anti–IFN-γ (clone XMG1.2). Samples were washed in PBS with 0.5% BSA before acquisition. Calculation of absolute numbers of different cell populations was performed by adding in each vial a fixed number (10,000) of nonfluorescent 10-μm polybead carboxylate microspheres (Polysciences, Niles, IL) according to the formula: Nb of cells = (Nb of acquired cells × 10,000)/(Nb of acquired beads). The number of cells obtained for each sample was extrapolated to the whole organs.

In Vivo Proliferation Assay

CD45.1 OTI T cells were incubated for 10 minutes at 37°C in PBS with 5 mM carboxyfluorescein diacetate succinimidyl ester (CFSE; Molecular Probes, Invitrogen, Cergy Pontoise, France). Cells (5 × 10^6) were injected in PBS into CD45.2 tumor-bearing or tumor-free mice. After 4 days, the frequency and number of OTI T cells that had performed more than three divisions (defined as highly divided) in axillary lymph nodes and tumor were measured while gating on CD45.1$^+$CD8$^+$ cells.

In Vitro Proliferation Assay

CD11c$^+$ cells were isolated from either MCA or MCA-OVA tumors of CP-treated or untreated mice using magnetic beads according to the manufacturer's instructions (Miltenyi Biotec; CD11c purity was above 80%). After purification, CD11c$^+$ cells (5 × 10^4) and CFSE-labeled naïve OTI T cells (10^5) were incubated in flat 96-well plate. After 3 days of coculture, cells were harvested and stained for flow cytometry analysis with anti-CD69 and anti-CD8 antibodies.

Multiphoton Imaging

Fluorescent OTI T cells (5 × 10^6) were injected i.v. Imaging experiments on tumors were performed 4 or 7 days after adoptive transfer. Tumors were carefully explanted from a skin flap. The thin fat layer was removed from the peritoneal side of the tumor to directly access the tumor parenchyma. Accessibility to the tumor parenchyma was evaluated by imaging an MCA-OVA tumor transfected with a yellow fluorescent protein (YFP)-encoding plasmid (see Figure 2D). Tumors were immobilized in an imaging chamber perfused with oxygenated (95% O_2 plus 5% CO_2) RPMI medium containing 10% fetal calf serum. The local temperature was monitored and maintained at 37°C. Dead cell staining was performed by a slow intratumoral injection of 50 μl of PBS with 1 mg/ml 4′, 6-diamidino-2-phenylindole, dihydrochloride (DAPI), at a distance from the analyzed area. We considered for imaging, peripheral areas of the tumor parenchyma in which OTI T cells were infiltrated disregarding the potential variability in the ratio between stromal cells and tumor cells. We assume that these regions are, however, representative to evaluate OTI T cell infiltration. For EL4 tumor, intravital imaging was performed on mouse kidney 18 days after tumor inoculation of CD11c-YFP mice. Briefly, mice were anesthetized with 2.5% isoflurane vaporized in a 70/30 mixture of O_2/N_2O. Kidneys were immobilized and exposed using a custom-made stereotactic holder. Mouse temperature was monitored and maintained at 37°C. Renal tubules were defined according to their autofluorescence and by i.v. Hoechst injection (50 μg in PBS) previous to imaging session.

The two-photon laser scanning microscopy (TPLSM) setup used was a Zeiss LSM 710 NLO multiphoton microscope (Carl Zeiss, Le Pecq, France) coupled to a Ti/sapphire crystal laser (Coherent ChameleonU, Santa Clara, CA) that provides 140-fs pulses of near-infrared (NIR) light, selectively tunable between 680 and 1080 nm, and an acousto-optic modulator to control laser power. The system included three external non-descanned detectors in reflection, which allow the simultaneous record of three fluorescent channels using a combination of two dichroic mirrors (565 and 690 nm) with 565/610 (DsRed) and 500/550 (YFP) band-pass filters and 485 low-pass filter (CFP, SHG, DAPI, Hoechst). The excitation wavelength was 870 nm. Cell motility was measured every 30 seconds by six consecutive 5-μm z spacing stacks using a plan apochromat ×20 (NA = 1) water immersion objective. For volume rendering movies, 1- to 3-μm z spacing stacks were performed, and three-dimensional (3D) reconstruction and volume rendering program from Imaris software (Bitplane, Zurich, Switzerland) were applied. For T cell tracking, images were average-projected and T cell motility parameters (previously defined [23]) were calculated using automatic tracking with manual correction using Imaris software. Cells that could not be tracked for more than 2 minutes were not considered. The arrest coefficient is defined as the proportion of time each cell's instantaneous velocity (calculated for every 30-second interval) is lower than 2 μm/min. The cell straightness corresponds to the ratio of the distance between the initial and the final positions of each cell to the total distance covered by the same cell. Quantification of OTI/CD11c$^+$YFP cell interactions was manually characterized according to the following criteria: 1) "stable" contact, defined by OTI T cell making contact with the same YFP$^+$ cell lasting all the imaging periods; 2) "confined" contact, defined by a single OTI making motile contact with one or more YFP$^+$ cells present in close vicinity; 3) "distant" contact, defined by a single OTI making sequential contacts with at least two different distant YFP$^+$ cells. The acquisition and analysis protocols for all experimental conditions to be compared were identical.

Histologic Tumor Analysis

Sagittal sections in the middle of tumors was performed as described [23], fixed overnight in 4% PFA, frozen in Tissue-Tek OCT compound, and sectioned (5 μm) with a cryostat (Leica). Tumor sections were additionally stained with hematoxylin/eosin or DAPI. Quantification of T cell and TuDC densities was performed by automatic tracking using Imaris software. Distance measurement was performed manually using Imaris software. The acquisition and analysis protocols for all images were identical.

Statistical Analysis

Two-way analysis of variance (ANOVA) was performed to compare tumor growth. For other comparisons, one-way ANOVA test was first performed, when significant, two by two Mann-Whitney rank sum tests were then performed to compare highly skewed distributions (typically, intravital analysis of cell behavior), and unpaired Student's t tests were used to compare Gaussian-like distributions (typically, flow cytometric analysis of numbers and frequencies of cell populations). Spearman test was performed for correlation analysis (symbols used: *P < .05; **P < .01; ***P < .001; NS, not significant).

Results

Chemotherapy Increases TIL Infiltration but Transiently Controls Tumor Growth

Ectopic tumors expressing model antigens such as OVA usually develop into highly immunogenic tumors for which the transfer of OVA-specific T cells confers tumor rejection. We have previously

described [22,24] a methylcholanthrene-induced fibrosarcoma cell line (MCA101) expressing OVA (MCA-OVA) that grows as solid subcutaneous syngeneic tumor after inoculation in C57Bl/6 mice. Injection of anti-OVA transgenic CD8$^+$ T cells (OTI T cells) 10 days after tumor inoculation was unable to control the rate of tumor growth, in accordance with a potent immunosuppressive environment induced by the tumor (Figure 1A). To overcome the immunosuppressive barrier, we performed intraperitoneal injection of CP at 100 mg/kg, 7 days after tumor inoculation. Single injection of CP led to a significant reduction in tumor growth in treated compared to untreated mice ($P < .001$; Figure 1A). Adoptive transfer of naïve OTI T cells, 3 days after chemotherapy, induced a more pronounced reduction in tumor growth (Figure 1A). Between days 10 and 18, OTI T cell transfer significantly reduced the percent change of tumor volume, but after day 18, the percent change was similar for all conditions, suggesting that tumor growth control by OTI T cells was only transient (Figure 1B). Analysis of OTI priming in tumor-draining lymph node revealed that CP treatment induced a significant increase in both the proliferation rate of OTI T cells and their IFN-γ production after *in vitro* restimulation with their cognate antigen (Figure W1). This increased expansion was associated with enhanced OTI infiltration into the tumor in CP-treated compared to untreated animals (Figure 1C) and with an increased ability to produce IFN-γ after *in vitro* restimulation with cognate antigen (Figure 1D). Despite an increased number and frequency of infiltrating OTI T cells after CP treatment, the frequency of IFN-γ–producing OTI T cells after *in vitro* restimulation was significantly impaired

between days 4 and 7 after transfer (Figure 1D), suggesting tolerance induction of OTI T cells, in accordance with tumor growth relapse.

CP Treatment Barely Affects the TuDC Network within the Tumor Parenchyma

To address the reasons why, despite efficient T cell priming and massive tumor infiltration, OTI T cells were unable to fully reject the tumor after chemotherapy, we characterized the myeloid cell compartment within the tumor. Tumor infiltrating CD11b$^+$Ly6G$^-$ myeloid cells expressed both CD11c and F4/80 markers, suggesting a strong overlap between TAM and TuDC populations (Figure 2A). Engelhardt et al. recently used the transgenic CD11c-YFP mouse strain to define TuDCs as a specific subpopulation of TAMs [19]. Two subsets of myeloid CD11b$^+$Ly6G$^-$ cell populations were distinguished in MCA-OVA tumor according to YFP expression that we designated TuDCs for YFP$^+$ myeloid cells and TAMs for YFP$^-$ cells, as proposed by Engelhardt et al. [19]. Extensive phenotyping in MCA-OVA tumors showed that TuDCs were CD11c^{high}F4/80^{high}Ly6c^{low} major histocompatibility complex (MHC) class II IAb$^+$ but also expressed more Mgl1 and IL4Rα. The TAM population was much more heterogeneous, including mature Ly6C^{low} and immature Ly6C^{high} macrophages [25,26] and displayed lower CD11c and I-Ab expression (Figure 2B). The TAM compartment increased after CP treatment corresponding to the infiltration of the Ly6C^{high} subset, whereas the number of TuDCs was apparently not modified. Nevertheless, a slight difference in Ly6C and F4/80 expression by TuDCs was observed in mice treated by CP compared to untreated mice, suggesting a rapid turnover of TuDCs
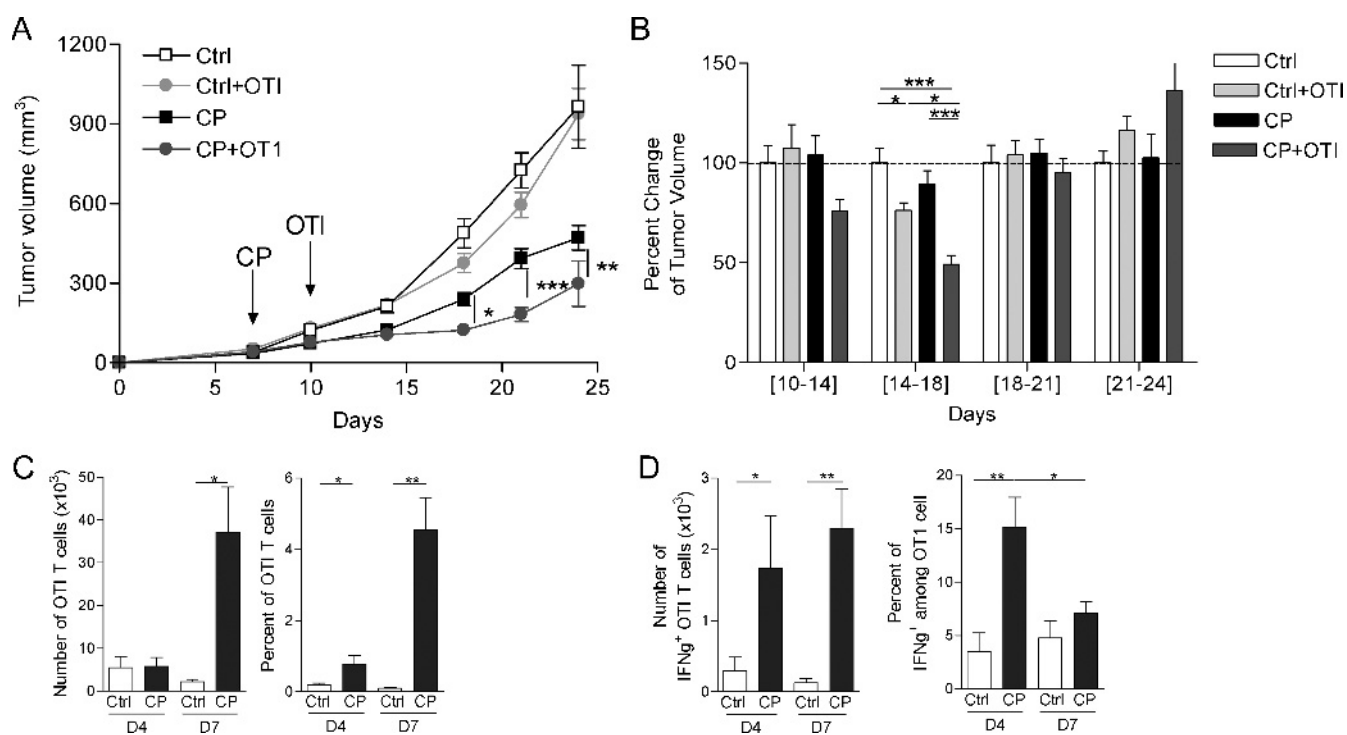

Figure 1. Chemotherapy increases TIL infiltration but transiently controls tumor growth. (A) MCA-OVA tumor cells were inoculated in the flank of C57Bl6 mice and tumor growth was monitored. Intraperitoneal injection of CP (100 mg/kg) was performed at day 7 and naïve OTI T cells were adoptively transferred at day 10. Graphs represent mean ± SEM tumor volume of 15 to 20 mice in each group pooled from four independent experiments. (B) Graph represents percent change in tumor growth determined by normalizing to Ctrl values, the fold increase of tumor volume during the indicated periods. Statistical analyses (ANOVA and Bonferroni post *t* test) were performed on raw data. (C–D) Graphs represent percent and absolute number of CD45.1 OTI T cells (C) and IFN-γ–producing CD45.1 OTI T cells (D) within the tumor. Bars represent mean ± SEM from at least five mice of two to four independent experiments.
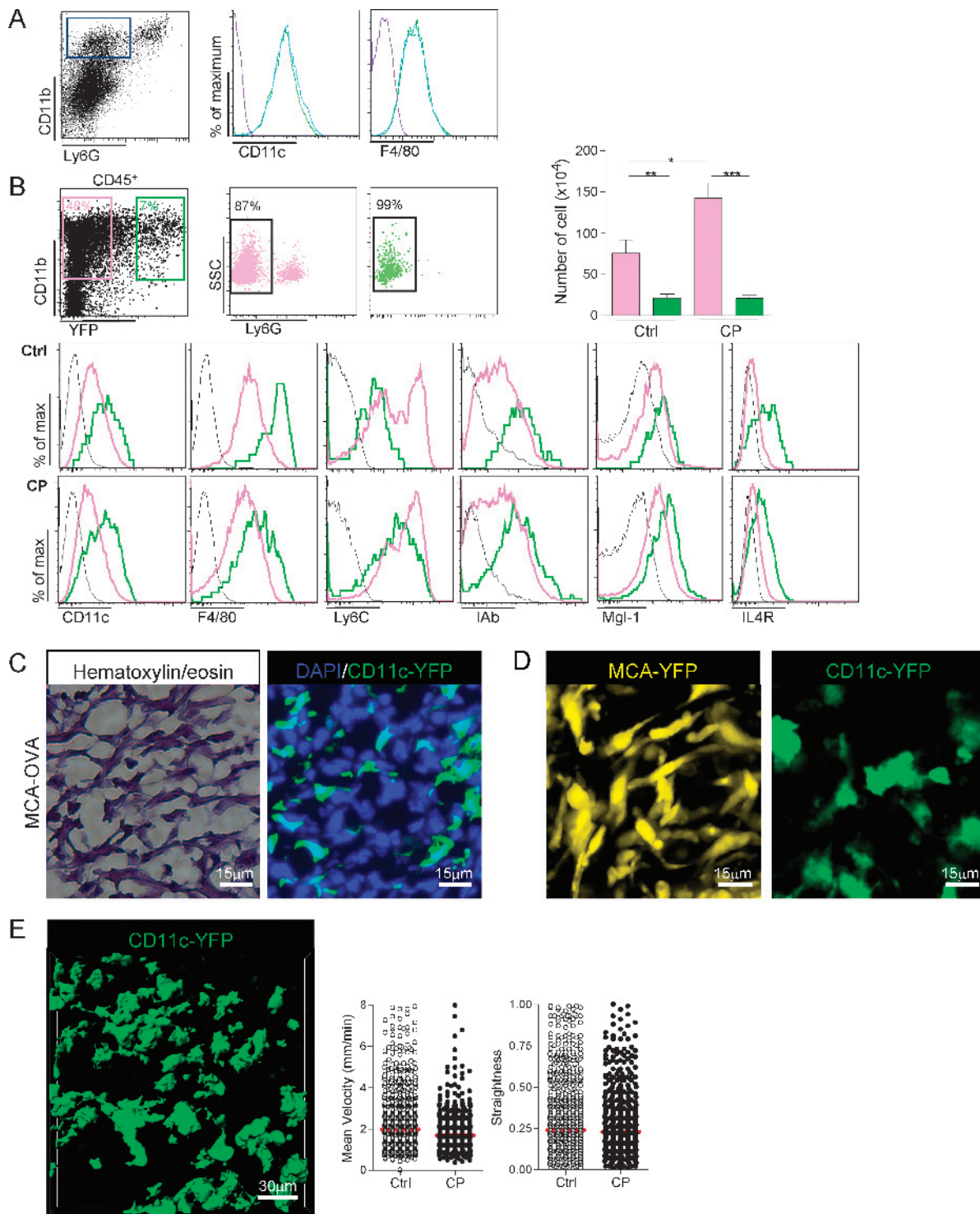
Figure 2. CP treatment barely affects the TuDC network within the tumor parenchyma. (A) Representative overlay histogram plot of CD11c and F4/80 expression gated on CD11b$^+$Ly6G$^-$ myeloid cells within the MCA-OVA tumors, 7 days after CP treatment (blue) or without treatment (green). Isotype staining is represented (purple). (B) Comparative multiparametric flow cytometric analysis of CD45$^+$CD11b$^+$YFP$^-$ (TAMs, pink) and CD45$^+$CD11b$^+$YFP$^+$ cells (TuDCs, green) from MCA-OVA tumors, 10 days after CP treatment or not. Bars represent the number of indicated cell populations (bars represent mean ± SEM from 9 to 16 mice of three independent experiments). (C) Representative hematoxylin/eosin staining (left) and fluorescent image (right) of frozen MCA-OVA tumor section from CD11c-YFP transgenic tumor-bearing mice. (D) Representative TPLSM images of an explanted MCA-OVA tumor transiently transfected with a YFP-encoding plasmid (left) and an MCA-OVA tumor inoculated in a CD11c-YFP transgenic mouse (right). (E) Volume rendering image (Movie W1) of an MCA-OVA tumor from a CD11c-YFP mouse. Graphs represent the quantification of YFP$^+$ velocity and straightness, 10 days after CP treatment or not. Red bar represents the median ($n = 822$ and $n = 547$ for Ctrl and CP-treated mice pooled from at least two independent experiments).

arising from the CP-mediated mobilization of Ly6C^{high} subset (Figure 2B). Histologic images (Figure 2C) and TPLSM images (Figure 2D) showed that TuDCs were distributed within the whole tumor parenchyma. Real-time imaging of the tumor in CD11c-YFP transgenic mice showed that TuDCs were slowly motile (mean velocity V_{mean} = 2.4 ± 1.6 µm/min) and displayed reduced displacements (straightness = 0.3 ± 0.2; Movie W1 and Figure 2E). TuDCs were however very dynamic with intense protrusive activity and performing several interconnections constituting a mesh (Movie W1). CP treatment did not affect the behavior of the TuDCs (Figure 2E).

In conclusion, CP treatment induces strong infiltration of immature macrophages but barely affects the TuDC network.

OTI T Cells Make Ag-dependent Interactions with TuDCs

To characterize the dynamic of TuDC and OTI T cell interactions within the tumor, MCA-OVA and MCA tumors were inoculated in a contralateral manner into CD11c-YFP mice. We used two-photon microscopy to monitor, 4 days after adoptive transfer, OTI T cell be-

havior in explanted tumors (Figure 3A and Movies W2–W3). In CP-treated as well as untreated mice, OTI T cells and YFP$^+$ cells were found in close proximity throughout the tumor parenchyma. Short movies with increased spatial resolution and volume rendering program confirmed that OTI T cells performed direct contacts with YFP$^+$ cells (Movies W4–W5). The OTI T cell arrest coefficient was higher in MCA-OVA compared to MCA tumors showing that OTI T cell made antigen-specific arrest on either tumor cells or TuDCs (Figure 3B). CD11c$^+$ cells isolated from MCA-OVA tumors cross-primed naïve OTI T cells in vitro, confirming that TuDCs were presenting the cognate antigen OVA$_{257–264}$ (Figure W2). We thus performed individual characterization of OTI T cells and defined three different types of contacts with YFP$^+$ cells: 1) "stable" contacts, defined by OTI T cell making contact with the same YFP$^+$ cells and lasting all the imaging periods; 2) "confined" contacts, defined by transient contacts with one or more YFP$^+$ cells present in close vicinity; 3) "distant" contacts, defined by sequential contacts with at least two different distant YFP$^+$ cells (Movie W6 and Figure 3C). In both CP-treated and untreated mice, up to 70% of
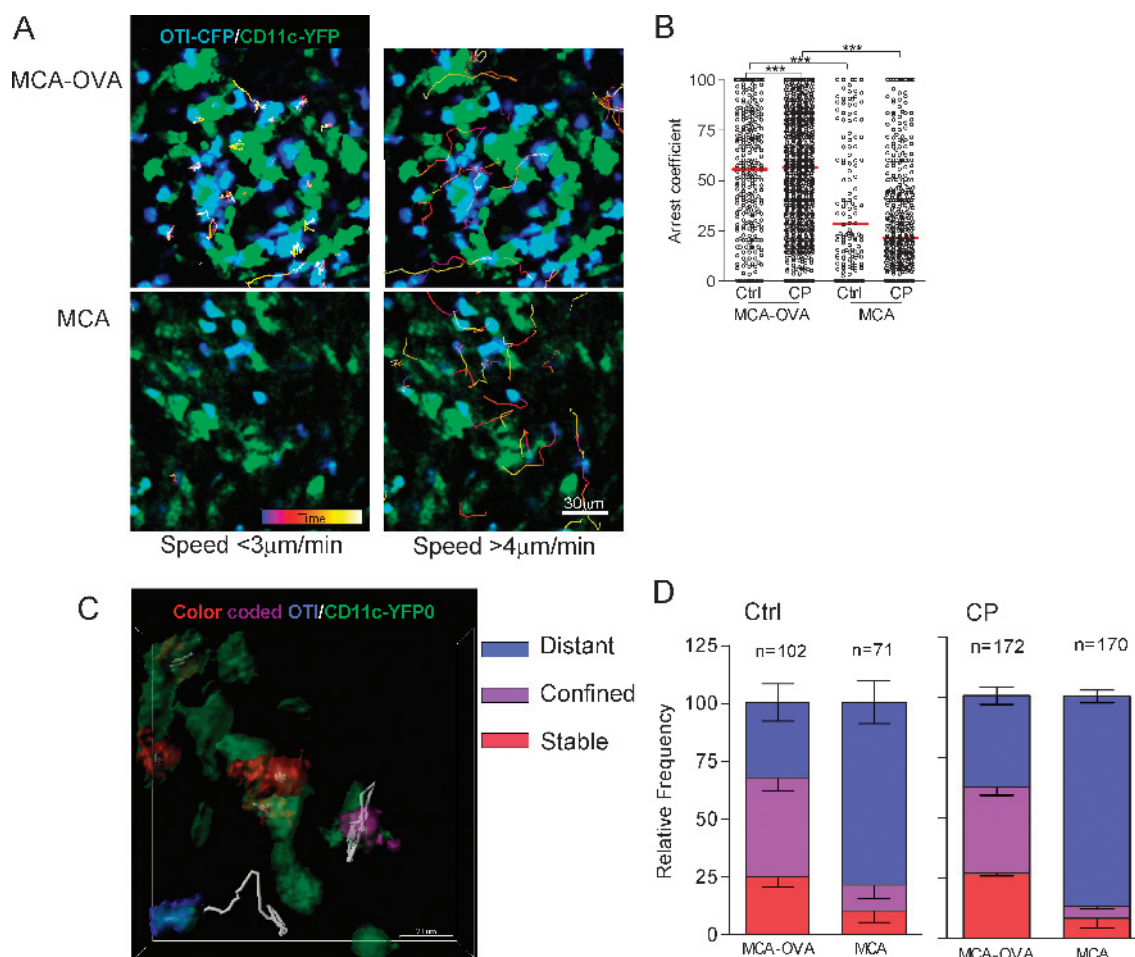

Figure 3. OTI T cells make Ag-dependent interactions with TuDCs. (A) Representative TPLSM images of OTI T cells (cyan) and YFP$^+$ stromal cells (green) within an MCA tumor and an MCA-OVA tumor, 4 days after OTI-CFP T cell adoptive transfer in a CP-treated CD11c-YFP–transgenic mouse. Track paths of OTI T cell moving at the indicated mean velocity are shown colored according to the time of imaging (color-coded time bar is shown). (B) Quantification of OTI T cell arrest coefficient (MCA Ctrl, n = 137; CP, n = 419 and MCA-OVA Ctrl, n = 271; CP, n = 920). Mann-Whitney statistical significances are indicated (upper right). (C) Volume rendering reconstitution image shows three representative OTI T cells colored according to the type of interaction performed with YFP$^+$ cells. OTI T cell track paths are represented in white. (D) Quantification of the relative frequency of the three types of OTI T cell/YFP$^+$ cell interactions. Bars represent mean ± SD of the relative frequency of the three types of interactions in each movie (three to four different movies have been evaluated for each condition). Total numbers of OTI T cell characterized are indicated.
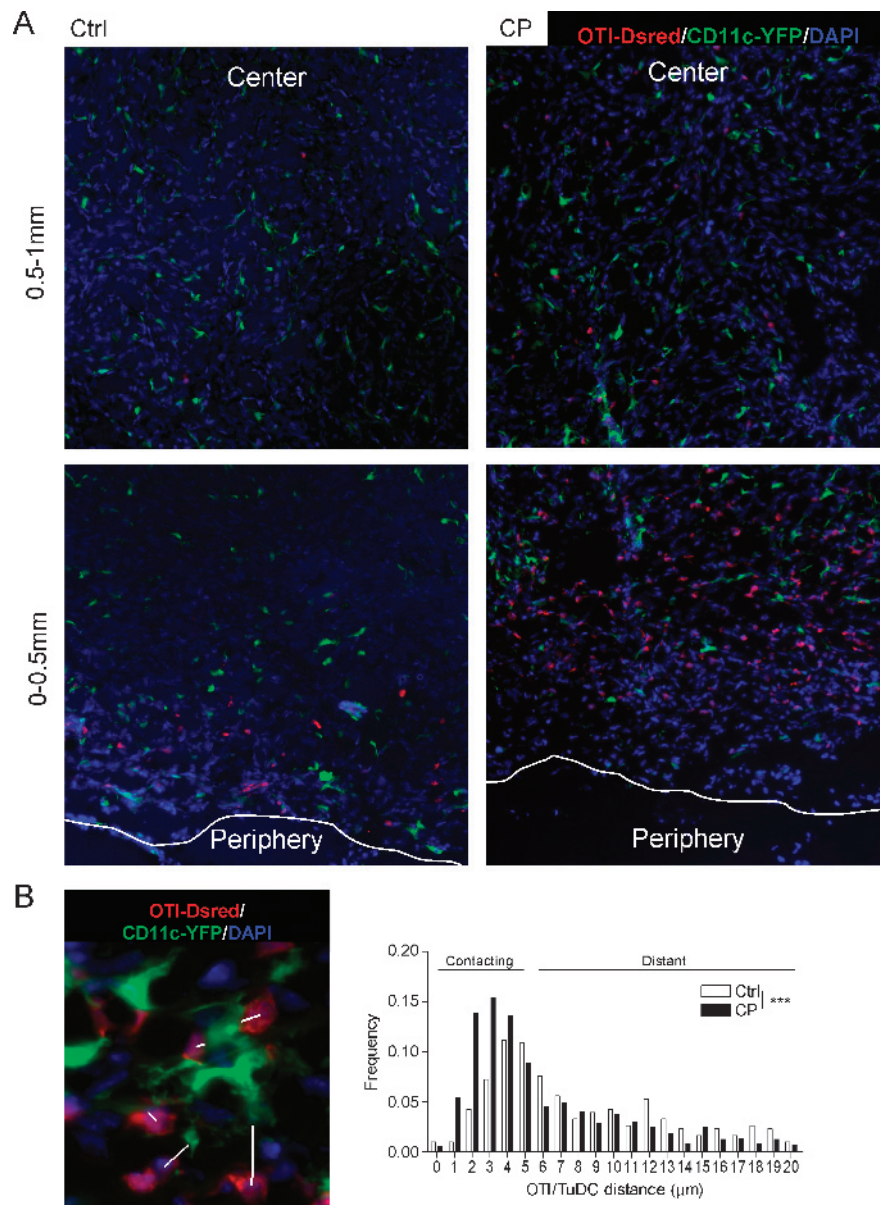
Figure 4. The proportion of TILs contacting TuDCs is enhanced after chemotherapy. OTI-DsRed T cells were adoptively transferred into CD11c-YFP transgenic mice bearing MCA-OVA tumor treated or not with CP. Seven days after adoptive transfer, tumors were carefully orientated and sectioned to define the periphery and the center of the tumor. (A) Representative tumor sections are shown and the distance from the periphery is indicated. OTI T cells are red, YFP$^+$ cells are green, and tumor parenchyma is stained by DAPI (blue). (B) Representative examples of the OTI T cell/YFP$^+$ distance measurement (white bars) between the center of the T cell and its proximal YFP$^+$ cell. Graph represents the frequency distribution of the distances (right). Mean radius of OTI T cell is 5 μm, and conjugates with a distance less than 5 μm are considered as contacting cells [n = 304 OTI cells for Ctrl (white bars) and n = 880 OTI cells for CP-treated mice (black bars) pooled from two to three different tumors].

OTI T cells made more stable and confined contacts with YFP$^+$ cells in MCA-OVA compared to 22% in MCA tumors (Figure 3D). We conclude that OTI T cells make antigen-specific interactions with TuDCs and that chemotherapy does not affect this behavior.

To evaluate whether the TIL/TuDC interactions characterized could be observed in another tumor model, we used the EL4 thymoma injected i.v. to C57Bl6 mice. EL4 cells spontaneously localize to several organs such as kidney and liver, where they develop into tumor nodules and induce animal death between 18 and 27 days (Figure W3A). Unfortunately, the OVA-expressing EL4 cell line is strongly immunogenic and was fully rejected when injected i.v. To examine CD8$^+$ T cell in-

filtration, we adoptively transferred purified polyclonal CD8$^+$ T cells from the lymph nodes of naïve Actb-DsRed/BL6 mice, 3 days after EL4 cell injection into CD11c-YFP mice. We performed intravital imaging of tumor nodules in the kidney on anesthetized mice 18 days after tumor inoculation and quantified the interaction between TILs and TuDCs (Figure W3B and Movie W7). Eighty percent of kidney-infiltrating CD8$^+$- DsRed TILs made interactions with TuDCs. Up to 60% were stable or confined similarly to antigen-specific interactions observed in the MCA-OVA tumors (Figure W3C). We conclude that preferential TIL interactions with TuDCs are applicable to several kinds of tumors.

The Proportion of TIL Contacting TuDC Is Enhanced after Chemotherapy

Two-photon imaging allows the visualization of only peripheral areas of the tumor. Thus, we further evaluated by histologic analysis on orientated sections of MCA-OVA tumors (as described [23]) the proportion of OTI T cell in contact with TuDCs, 7 days after adoptive transfer at the time tolerance was induced. In untreated mice, OTI T cells were only located at the periphery compared to CP-treated mice for which OTI T cells infiltrated in higher number and in deeper regions of the tumor (Figure 4A). Considering that the mean radius of OTI T cells is 5 μm, quantification of the distance between the center of OTI T cell and the nearest TuDC showed that 29% and 54% of OTI T cells were in contact (less than 5 μm) with YFP+ cells in untreated and CP-treated mice, respectively (Figure 4B). Thus, the proportion of TILs contacting TuDCs is enhanced after chemotherapy.

TIL Infiltration Is Stopped in TuDC-Rich Areas

We hypothesized that TuDC network would influence OTI T cell infiltration after CP treatment. Seven days after adoptive transfer, peripheral regions of the tumor were filled by collagen fibers (Figure 5A). DAPI injection revealed that collagen-rich areas were full of dead cells (Figure 5B). Analysis of T cell motility confirmed that in "collagen-rich" regions, T cells displayed higher velocity and straightness compared to "TuDC-rich" areas (Figure 5C and Movies W8–W9), suggesting that OTI T cells were trapped by TuDC network.

TILs Are Trapped in TuDC Network

To address the question of whether TuDCs retained OTI T cells, we performed histologic analysis of the distribution of OTI T cells and YFP+ cells. Quantification of the YFP+ cell density on histologic section, 7 days after adoptive transfer (Figure 6A), clearly showed a positive correlation between the density of OTI T cells and YFP+ cells in subregions of the tumor (Figure 6B). We conclude that OTI T cells are trapped by TuDCs through antigen-specific interactions, restricting their infiltration into the whole tumor parenchyma.

Discussion

Conventional chemotherapies provide clinically interesting immunostimulatory outcomes, but most often, effects are transient and fail because of the tumor-induced immunosuppressive environment. TAMs are the main protagonists involved in T cell immunosubversion [18]. They are represented by a very heterogenous and plastic population
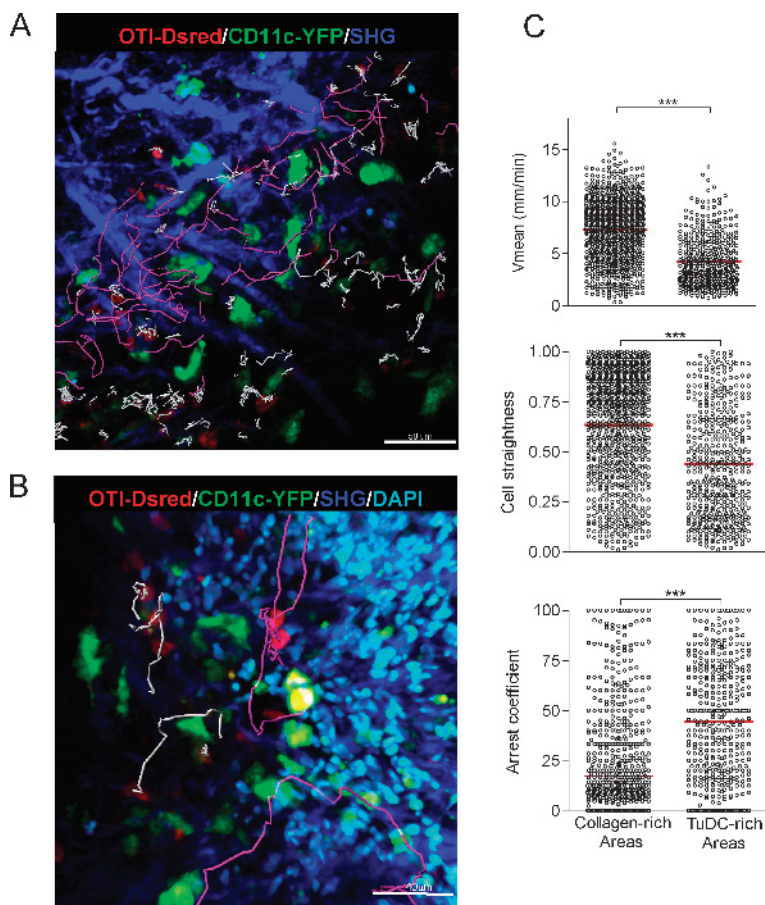

Figure 5. TIL infiltration is stopped in TuDC-rich areas. (A) TPLSM image showing collagen fibers (blue), YFP+ cells (green), and OTI T cells (red) in the peripheral area of an MCA-OVA tumor from a CP-treated mouse. Representative track paths of OTI T cell with a straightness of >0.5 are indicated in purple and those with a straightness of <0.5 are in white. (B) TPLSM image after DAPI injection (cyan). Representative track paths of OTI T cell in DAPI-rich area are indicated in purple and those in TuDC-rich area are in white. (C) Graphs represent the quantification of OTI T cell velocity, straightness, and arrest coefficient, 7 days after OTI T cell adoptive transfer in CP-treated mice (data are pooled from at least three independent experiments). Red bar represents the mean. Mann-Whitney statistical significances are indicated.
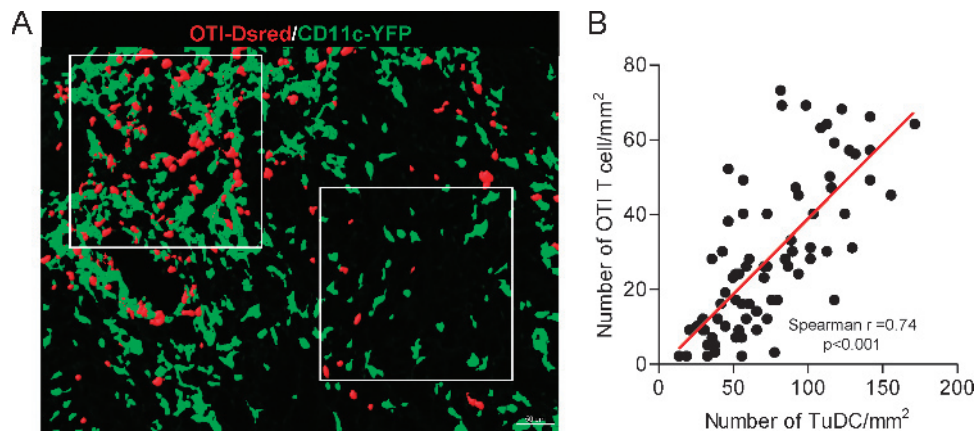
Figure 6. TILs are trapped in TuDC network. OTI T cell and YFP$^+$ cell densities were quantified by histologic analysis 7 days after adoptive transfer of OTI-DsRed T cell into CD11c-YFP transgenic mice bearing MCA-OVA tumors treated with CP. (A) The image illustrates cell densities in 250-μm^2 fields (white square) after volume rendering. White squares were located by area with homogenous distribution of OTI T cells. (B) Each dot represents the density of OTI T cells as a function of the density of TuDCs. The numbers of red and green cells were determined automatically in 75 different fields from more than 20 images taken serially from the periphery to the center of the tumor, of three different tumors. Red line represents the linear regression. Spearman r and P value are indicated.

[27] and their frequency is associated with poor prognosis. Despite preferential localization of TAMs in hypoxic regions has been documented, their angiogenic, tissue remodeling, growth factor–providing, and immunosuppressive properties are required in the whole tumor parenchyma [28–30]. TuDCs also play a role in the subversion of adaptive immunity [18]. TuDCs share common markers with TAMs, and their phenotypic and functional distinction is still a matter of debate. Recently, Engelhardt et al. provided clear evidence in a new transgenic PyMT-MMTV strain that TuDCs display potent immunosuppressive activity toward adoptively transferred OTI T cells through stable engagement [19]. The role of TuDC in adaptive T cell immunosubversion after chemotherapy is less well documented.

After adoptive transfer into MCA-OVA–bearing mice, tumor-specific CD8$^+$ T cells were primed in the draining lymph node and infiltrated the tumor but failed to control tumor growth [24]. Mice preconditioning by CP treatment efficiently increased priming of T cells and tumor infiltration but had only a transient control in tumor progression associated with a rapid loss of effector functions. We deciphered antitumor-specific T cell infiltration after chemotherapy by following their interactions with TuDCs using two-photon real-time imaging technology on explanted tumor tissues. We used the CD11c-YFP transgenic mice and showed that YFP$^+$ cells were distributed in the whole parenchyma, exhibited reduced displacements but strong protrusive activity that allowed interconnections, and generated a network of ramified TuDCs like that described previously for macrophages [31]. CP induces dendritic cell (DC) precursor expansion and activation between 10 and 15 days after treatment, which correlates with increased T cell antitumor activity [32–36]. After CP treatment, we observed an accumulation of an immature Ly6C^{high} myeloid population in the YFP$^-$ myeloid cell compartment. The possible overlap of this Ly6c^{high} subset with the myeloid-derived suppressor cell Gr1$^+$ population may lead to confused interpretations and warrants caution. Nakasone et al. observed CCR2-dependent infiltration of myeloid cells after chemotherapy in a mammary carcinoma model and a delayed tumor relapse in CCR2-deficient mice [37], suggesting that after *de novo* infiltration of mobilized inflammatory monocytes, these last

converted into pro-tumoral myeloid cells. Increased Ly6C and reduced F4/80 expression on YFP$^+$ cell after CP treatment suggested that Ly6C^{high} myeloid subset also contributed to the renewal of TuDCs. The number of TuDCs was not affected by CP treatment, suggesting a controlled process of renewal. We next addressed whether this network of YFP$^+$ cells would impact T cell infiltration. Live imaging of the explanted tumor showed that OTI T cell more stably engage YFP$^+$ cells in MCA-OVA tumors compared to contralateral MCA tumors. These observations suggested that TIL/TuDC preferential interaction was due to the availability of antigen rather than other nonspecific receptor/ligand recognition. Up to 54% of OTI T cells were in close contact with YFP$^+$ cells in CP-treated animals, 7 days after adoptive transfer, compared to 29% in control animals, suggesting that TIL/TuDC conjugates accumulated when tumor cells were partially eliminated. Colocalization of the two populations within the whole tumor parenchyma supported that OTI T cells were trapped by the TuDC network. The reasons why TuDCs were resistant to OTI T cell–mediated cell death will require further investigations. Increased doses of CP treatment improved the rejection of the tumor by OTI T cells (data not shown) and emphasized myeloablation, suggesting that destruction of TuDCs by stronger and longer myeloablation would improve the T cell–mediated rejection. We observed that the trapping of TILs within the TuDC network could be also observed in an aggressive model of secondary tumor localization in the kidney, suggesting that trapping of TILs is applicable to different tumors. In this *in vivo* imaging system, we observed that TIL and TuDC interactions were similar to those observed in explanted MCA-OVA tumors, suggesting that the explanted tissue procedure does not affect the interaction. We could not confirm that red fluorescent CD8$^+$ T cells within the tumor were antigen-specific. Nevertheless, no red fluorescent CD8$^+$ T cells could be detected in non–tumor-bearing mice (unpublished observation) and only activated cells are those that usually infiltrate the tumor.

We propose that despite strong antitumor effector activity induced by chemotherapy, TuDC networks trap T cells through antigen-subversive interactions leading to their tolerance. Our work provides
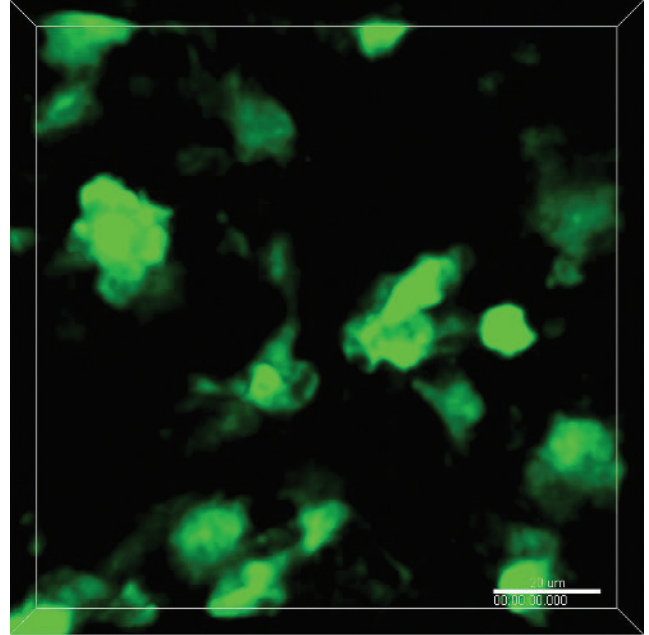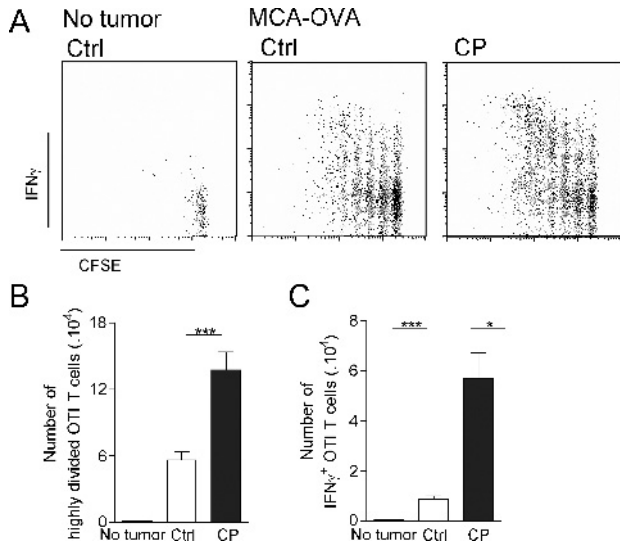
new insights into the spatiotemporal orchestration of TIL/TuDC interactions and provides perspectives for the improvement of anticancer chemotherapy.

Acknowledgments

References

[1] Ramakrishnan R, Antonia S, and Gabrilovich DI (2008). Combined modality immunotherapy and chemotherapy: a new perspective. *Cancer Immunol Immunother* **57**, 1523–1529.

[2] Schlom J, Arlen PM, and Gulley JL (2007). Cancer vaccines: moving beyond current paradigms. *Clin Cancer Res* **13**, 3776–3782.

[3] Dudley ME, Yang JC, Sherry R, Hughes MS, Royal R, Kammula U, Robbins PF, Huang J, Citrin DE, Leitman SF, et al. (2008). Adoptive cell therapy for patients with metastatic melanoma: evaluation of intensive myeloablative chemoradiation preparative regimens. *J Clin Oncol* **26**, 5233–5239.

[4] Apetoh L, Ghiringhelli F, Tesniere A, Obeid M, Ortiz C, Criollo A, Mignot G, Maiuri MC, Ullrich E, Saulnier P, et al. (2007). Toll-like receptor 4–dependent contribution of the immune system to anticancer chemotherapy and radiotherapy. *Nat Med* **13**, 1050–1059.

[5] Ghiringhelli F, Apetoh L, Housseau F, Kroemer G, and Zitvogel L (2007). Links between innate and cognate tumor immunity. *Curr Opin Immunol* **19**, 224–231.

[6] Garnett CT, Palena C, Chakraborty M, Tsang KY, Schlom J, and Hodge JW (2004). Sublethal irradiation of human tumor cells modulates phenotype resulting in enhanced killing by cytotoxic T lymphocytes. *Cancer Res* **64**, 7985–7994.

[7] Ramakrishnan R, Assudani D, Nagaraj S, Hunter T, Cho HI, Antonia S, Altiok S, Celis E, and Gabrilovich DI (2010). Chemotherapy enhances tumor cell susceptibility to CTL-mediated killing during cancer immunotherapy in mice. *J Clin Invest* **120**, 1111–1124.

[8] Luznik L, Jones RJ, and Fuchs EJ (2010). High-dose cyclophosphamide for graft-versus-host disease prevention. *Curr Opin Hematol* **17**, 493–499.

[9] Greenberg PD, Kern DE, and Cheever MA (1985). Therapy of disseminated murine leukemia with cyclophosphamide and immune Lyt-1$^+$,2$^-$ T cells. Tumor eradication does not require participation of cytotoxic T cells. *J Exp Med* **161**, 1122–1134.

[10] Dudley ME, Wunderlich JR, Robbins PF, Yang JC, Hwu P, Schwartzentruber DJ, Topalian SL, Sherry R, Restifo NP, Hubicki AM, et al. (2002). Cancer regression and autoimmunity in patients after clonal repopulation with antitumor lymphocytes. *Science* **298**, 850–854.

[11] Ghiringhelli F, Menard C, Puig PE, Ladoire S, Roux S, Martin F, Solary E, Le Cesne A, Zitvogel L, and Chauffert B (2007). Metronomic cyclophosphamide regimen selectively depletes CD4$^+$CD25$^+$ regulatory T cells and restores T and NK effector functions in end stage cancer patients. *Cancer Immunol Immunother* **56**, 641–648.

[12] Lutsiak ME, Semnani RT, De Pascalis R, Kashmiri SV, Schlom J, and Sabzevari H (2005). Inhibition of CD4$^+$25$^+$ T regulatory cell function implicated in enhanced immune response by low-dose cyclophosphamide. *Blood* **105**, 2862–2868.

[13] North RJ (1982). Cyclophosphamide-facilitated adoptive immunotherapy of an established tumor depends on elimination of tumor-induced suppressor T cells. *J Exp Med* **155**, 1063–1074.

[14] Berraondo P, Nouze C, Preville X, Ladant D, and Leclerc C (2007). Eradication of large tumors in mice by a tritherapy targeting the innate, adaptive, and regulatory components of the immune system. *Cancer Res* **67**, 8847–8855.

[15] Zitvogel L, Apetoh L, Ghiringhelli F, and Kroemer G (2008). Immunological aspects of cancer chemotherapy. *Nat Rev Immunol* **8**, 59–73.

[16] Pollard JW (2009). Trophic macrophages in development and disease. *Nat Rev Immunol* **9**, 259–270.

[17] Gabrilovich DI and Nagaraj S (2009). Myeloid-derived suppressor cells as regulators of the immune system. *Nat Rev Immunol* **9**, 162–174.

[18] Mantovani A, Sozzani S, Locati M, Schioppa T, Saccani A, Allavena P, and Sica A (2004). Infiltration of tumours by macrophages and dendritic cells: tumour-associated macrophages as a paradigm for polarized M2 mononuclear phagocytes. *Novartis Found Symp* **256**, 137–145; discussion 146-138, 259-169.

[19] Engelhardt JJ, Boldajipour B, Beemiller P, Pandurangi P, Sorensen C, Werb Z, Egeblad M, and Krummel MF (2012). Marginating dendritic cells of the tumor microenvironment cross-present tumor antigens and stably engage tumor-specific T cells. *Cancer Cell* **21**, 402–417.

[20] Lindquist RL, Shakhar G, Dudziak D, Wardemann H, Eisenreich T, Dustin ML, and Nussenzweig MC (2004). Visualizing dendritic cell networks *in vivo*. *Nat Immunol* **5**, 1243–1250.

[21] Restifo NP, Spiess PJ, Karp SE, Mule JJ, and Rosenberg SA (1992). A nonimmunogenic sarcoma transduced with the cDNA for interferon γ elicits CD8$^+$ T cells against the wild-type tumor: correlation with antigen presentation capability. *J Exp Med* **175**, 1423–1431.

[22] Zeelenberg IS, Ostrowski M, Krumeich S, Bobrie A, Jancic C, Boissonnas A, Delcayre A, Le Pecq JB, Combadiere B, Amigorena S, et al. (2008). Targeting tumor antigens to secreted membrane vesicles *in vivo* induces efficient antitumor immune responses. *Cancer Res* **68**, 1228–1235.

[23] Boissonnas A, Fetler L, Zeelenberg IS, Hugues S, and Amigorena S (2007). *In vivo* imaging of cytotoxic T cell infiltration and elimination of a solid tumor. *J Exp Med* **204**, 345–356.

[24] Boissonnas A, Scholer-Dahirel A, Simon-Blancal V, Pace L, Valet F, Kissenpfennig A, Sparwasser T, Malissen B, Fetler L, and Amigorena S (2010). Foxp3$^+$ T cells induce perforin-dependent dendritic cell death in tumor-draining lymph nodes. *Immunity* **32**, 266–278.

[25] de Bruijn MF, Slieker WA, van der Loo JC, Voerman JS, van Ewijk W, and Leenen PJ (1994). Distinct mouse bone marrow macrophage precursors identified by differential expression of ER-MP12 and ER-MP20 antigens. *Eur J Immunol* **24**, 2279–2284.

[26] Sunderkotter C, Nikolic T, Dillon MJ, Van Rooijen N, Stehling M, Drevets DA, and Leenen PJ (2004). Subpopulations of mouse blood monocytes differ in maturation stage and inflammatory response. *J Immunol* **172**, 4410–4417.

[27] Biswas SK and Mantovani A (2010). Macrophage plasticity and interaction with lymphocyte subsets: cancer as a paradigm. *Nat Immunol* **11**, 889–896.

[28] Condeelis J and Pollard JW (2006). Macrophages: obligate partners for tumor cell migration, invasion, and metastasis. *Cell* **124**, 263–266.

[29] Sica A, Larghi P, Mancino A, Rubino L, Porta C, Totaro MG, Rimoldi M, Biswas SK, Allavena P, and Mantovani A (2008). Macrophage polarization in tumour progression. *Semin Cancer Biol* **18**, 349–355.

[30] Allavena P, Sica A, Solinas G, Porta C, and Mantovani A (2008). The inflammatory micro-environment in tumor progression: the role of tumor-associated macrophages. *Crit Rev Oncol Hematol* **66**, 1–9.

[31] Caillou B, Talbot M, Weyemi U, Pioche-Durieu C, Al Ghuzlan A, Bidart JM, Chouaib S, Schlumberger M, and Dupuy C (2011). Tumor-associated macrophages (TAMs) form an interconnected cellular supportive network in anaplastic thyroid carcinoma. *PLoS One* **6**, e22567.

[32] Salem ML, Diaz-Montero CM, Al-Khami AA, El-Naggar SA, Naga O, Montero AJ, Khafagy A, and Cole DJ (2009). Recovery from cyclophosphamide-induced lymphopenia results in expansion of immature dendritic cells which can mediate enhanced prime-boost vaccination antitumor responses *in vivo* when stimulated with the TLR3 agonist poly(I:C). *J Immunol* **182**, 2030–2040.

[33] Nakahara T, Uchi H, Lesokhin AM, Avogadri F, Rizzuto GA, Hirschhorn-Cymerman D, Panageas KS, Merghoub T, Wolchok JD, and Houghton AN (2010). Cyclophosphamide enhances immunity by modulating the balance of dendritic cell subsets in lymphoid organs. *Blood* **115**, 4384–4392.

[34] Salem ML, Al-Khami AA, El-Naggar SA, Diaz-Montero CM, Chen Y, and Cole DJ (2010). Cyclophosphamide induces dynamic alterations in the host micro-environments resulting in a Flt3 ligand-dependent expansion of dendritic cells. *J Immunol* **184**, 1737–1747.

[35] Schiavoni G, Sistigu A, Valentini M, Mattei F, Sestili P, Spadaro F, Sanchez M, Lorenzi S, D'Urso MT, Belardelli F, et al. (2011). Cyclophosphamide synergizes with type I interferons through systemic dendritic cell reactivation and induction of immunogenic tumor apoptosis. *Cancer Res* **71**, 768–778.

[36] Salem ML, El-Naggar SA, and Cole DJ (2011). Cyclophosphamide induces bone marrow to yield higher numbers of precursor dendritic cells *in vitro* capable of functional antigen presentation to T cells *in vivo*. *Cell Immunol* **261**, 134–143.

[37] Nakasone ES, Askautrud HA, Kees T, Park JH, Plaks V, Ewald AJ, Fein M, Rasch MG, Tan YX, Qiu J, et al. (2012). Imaging tumor-stroma interactions during chemotherapy reveals contributions of the microenvironment to resistance. *Cancer Cell* **21**, 488–503.

Figure W1. CP treatment increases priming of OTI T cells in draining lymph node. (A) Representative CFSE dilution and IFN-γ production profile by CD45.1 OTI T cells in tumor draining lymph node (tdLN), 4 days after adoptive transfer into MCA-OVA tumor–bearing mice treated or not with CP and tumor-free mice. Quantification of the number of OTI T cells that have undergone more than three cell divisions (B) and that are producing IFN-γ (C), 4 days after adoptive transfer in CP-treated (black) or untreated (white) mice. Bars represent mean ± SEM of absolute numbers from at least nine mice of three independent experiments.

Movie W1. TuDCs make dynamic interconnections within the tumor parenchyma. Time-lapse TPLSM video showing YFP+ cells (green) within an MCA-OVA tumor explanted from a CD11c-YFP transgenic mouse.
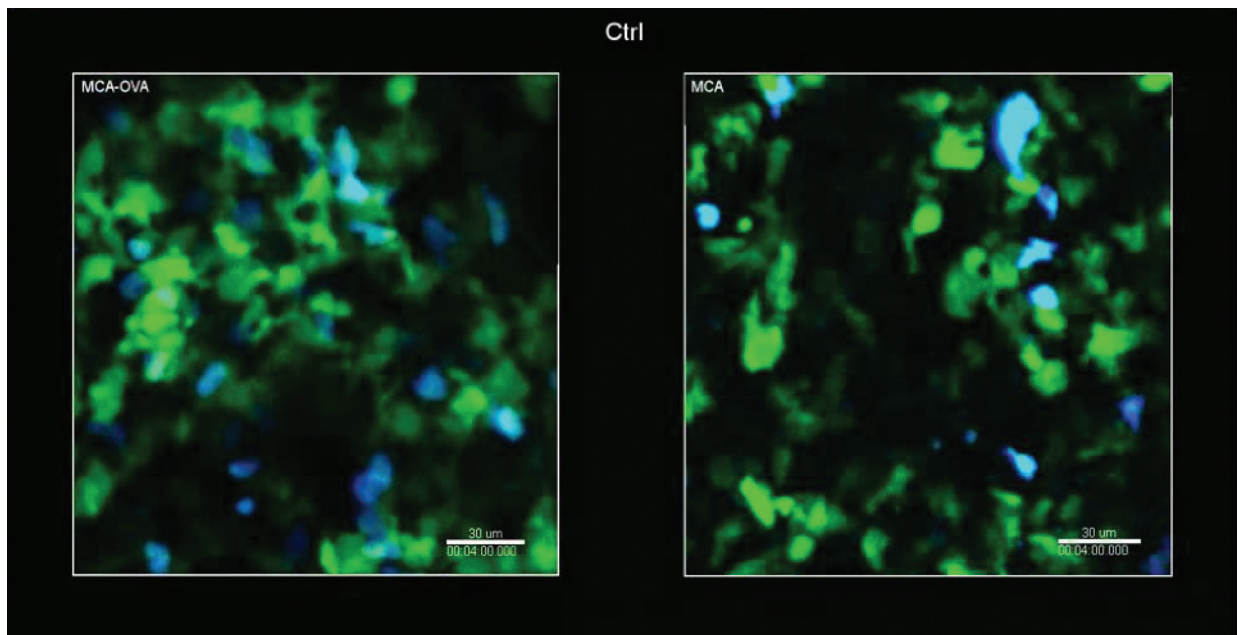
Movie W2. Antigen-specific OTI/TuDC interactions within untreated tumors. Montage of two time-lapse TPLSM videos showing OTI-CFP cells (cyan) and CD11c-YFP+ cells (green) within an MCA-OVA tumor (left) and an MCA tumor (right), 4 days after adoptive transfer in the absence of CP treatment.
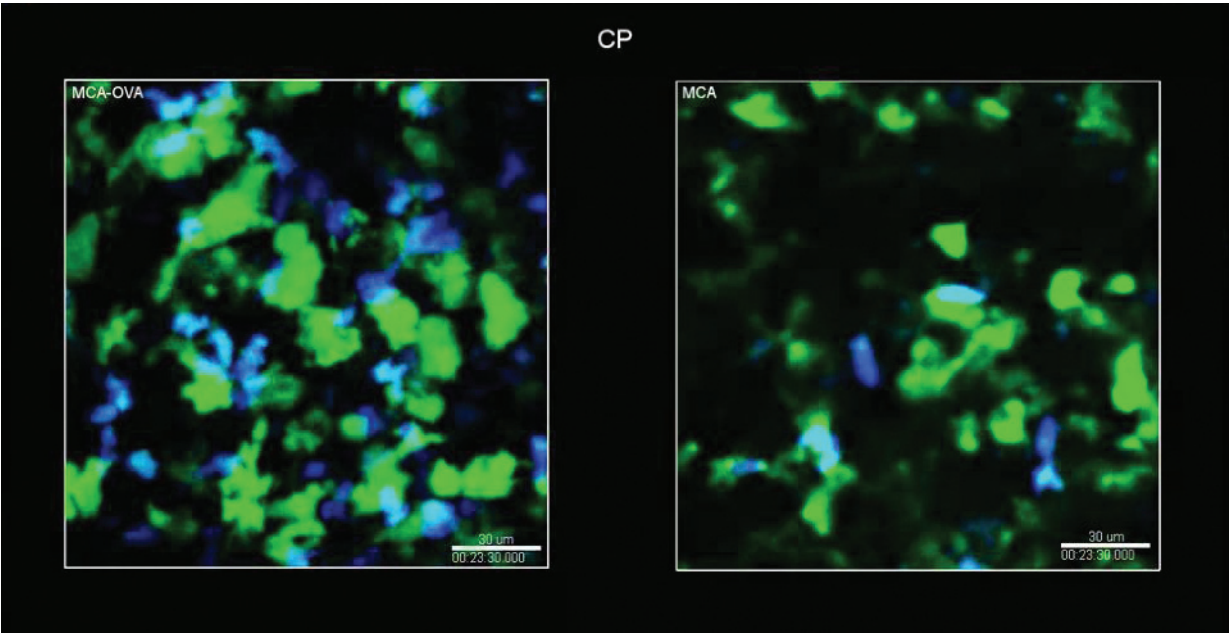
Movie W3. Antigen-specific OTI/TuDC interactions within CP-treated tumors. Montage of two time-lapse TPLSM videos showing OTI-CFP cells (cyan) and CD11c-YFP$^+$ cells (green) within an MCA-OVA tumor (left) and an MCA tumor (right), 4 days after adoptive transfer in a mouse treated with 100 mg/kg CP.
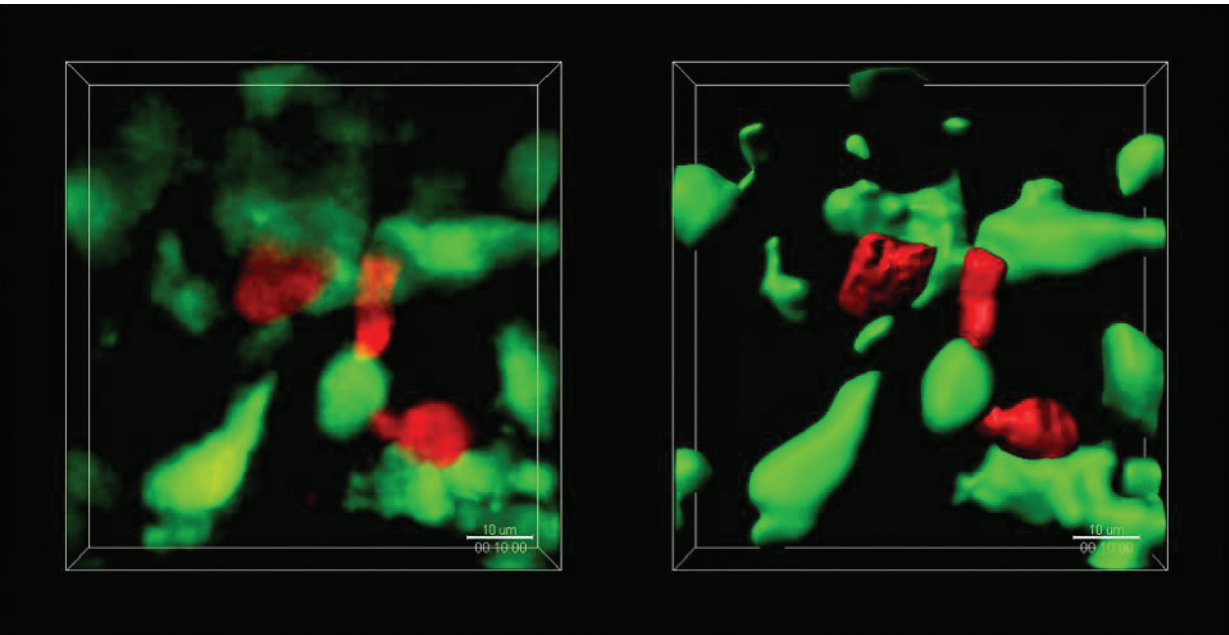
Movie W4. Volume rendering OTI/TuDC interactions. Montage of two time-lapse TPLSM 3D videos showing OTI-DsRed cell (red) and CD11c-YFP$^+$ cell (green) interactions within an MCA-OVA tumor before (left) and after (right) volume rendering.
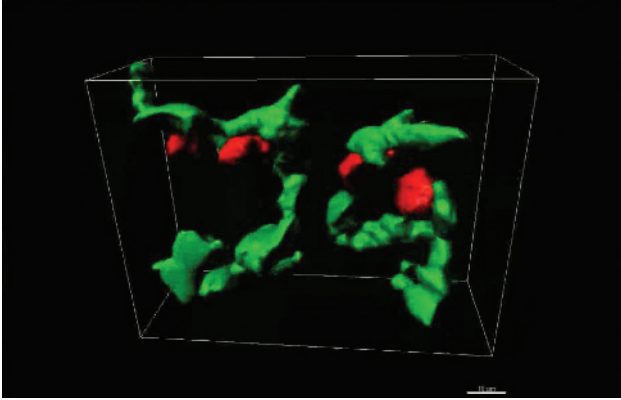
Movie W5. 3D reconstruction of volume rendering OTI/TuDC inter-actions. TPLSM 3D reconstruction of 1-μm z spacing stack showing OTI-DsRed cell (red) and CD11c-YFP$^+$ cell (green) interactions within an MCA-OVA tumor after volume rendering.
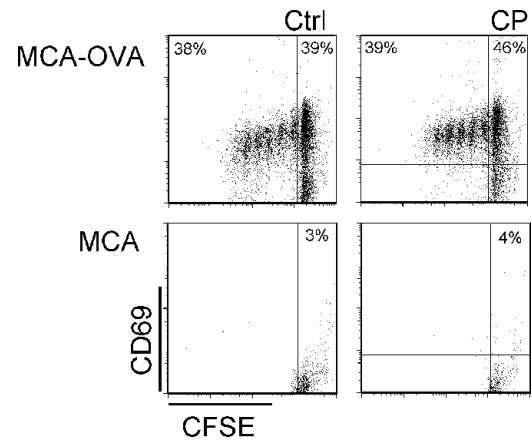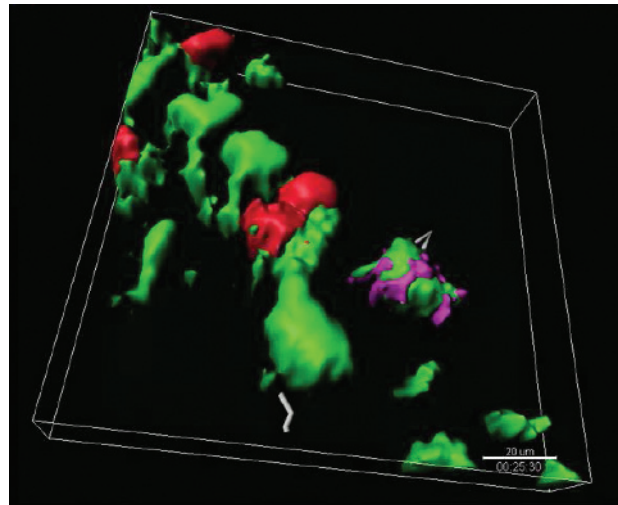
Figure W2. TuDCs cross prime OTI T cells. Representative dot plot of CD69 expression and CFSE dilution profile of OTI T cells 3 days after coculture with CD11c$^+$ cells isolated from MCA-OVA tumors (upper panels) or MCA tumors (lower panels) treated or not by CP. Results are representative of two independent experiments.

Movie W6. Volume rendering of distinct OTI/TuDC interactions. Time-lapse TPLSM 3D video showing different types of OTI-DsRed (colored) and YFP$^+$ (green) cell interactions after volume rendering. Blue represents distant contact, purple represents confined con-tact, and red represents stable contacts. OTI T cell track paths are displayed in white.
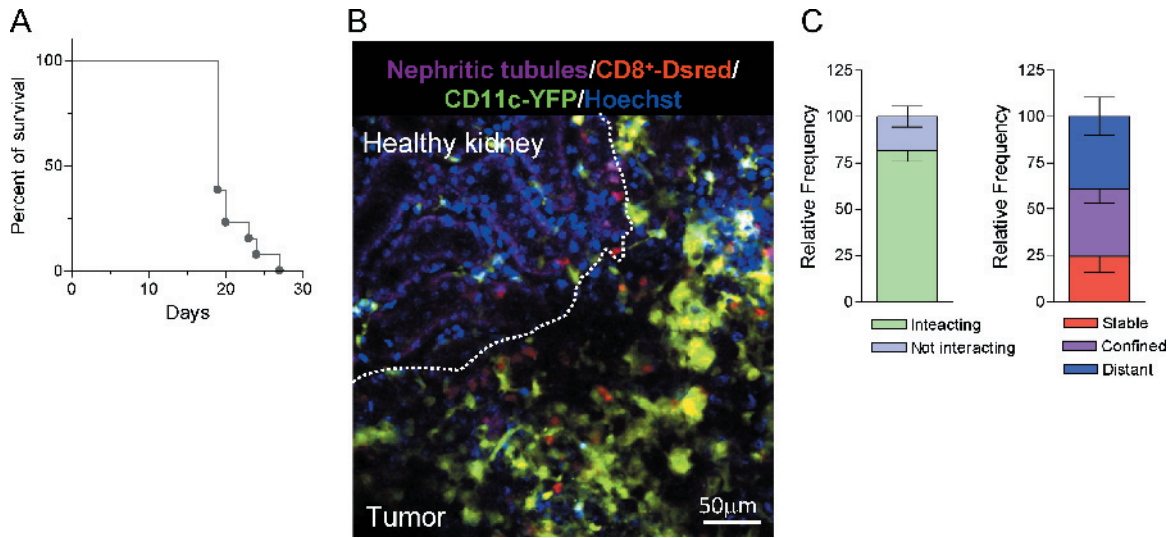
Figure W3. TILs interact with TuDCs of renal tumor. (A) EL4 tumor cells were inoculated i.v. into C57Bl6 mice and survival was monitored. Kaplan-Meier survival curve represents a pool of 13 mice of three independent experiments. (B) TPLSM image showing CD8$^+$-DsRed T cells (red), CD11c-YFP$^+$ cells (yellow), and autofluorescent renal tubules (purple) within an EL4-kidney tumor, 18 days after tumor cell injection. Nucleus staining (blue) is performed by i.v. injection of Hoechst (50 μg in PBS) before imaging. White dashed line delimits the healthy kidney and the tumor nodule. (C) Quantification of the proportion of OTI T cells interacting with YFP$^+$ cells and the relative frequency of the different types of OTI/YFP$^+$ cell interactions. Bars represent mean $\pm$ SD from eight different movies of three different mice. Total T cells quantified is $n = 334$.
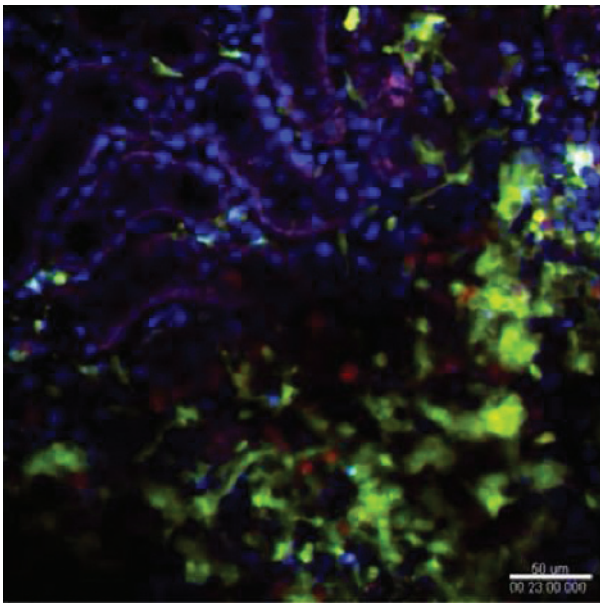
Movie W7. TIL and TuDC interactions in EL4-kidney tumor. Time-lapse TPLSM video showing CD8$^+$-DsRed T cells (red) and CD11c-YFP$^+$ cells (yellow) within an EL4-kidney tumor, 18 days after i.v. injection. Nucleus staining (blue) of autofluorescent renal tubules (purple) is performed by i.v. injection of Hoechst (50 μg) before imaging.
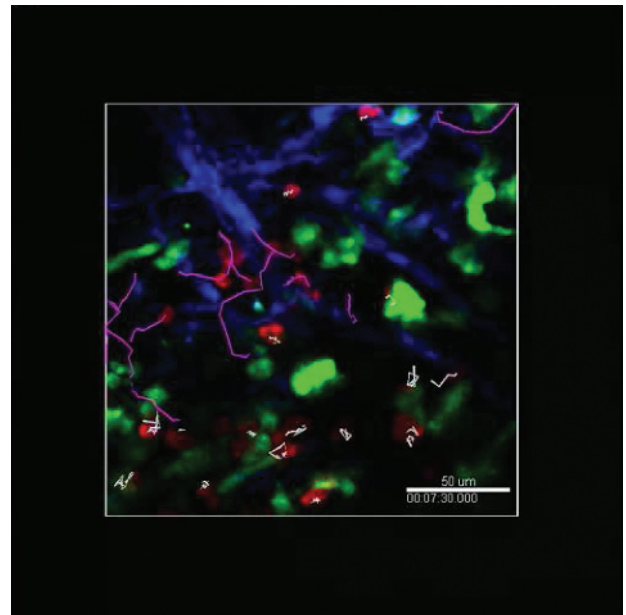
Movie W8. OTI T cell dynamics in different regions of the tumor. Time-lapse TPLSM video showing OTI-DsRed cells (red), CD11c-YFP$^+$ cells (green), and collagen fibers (SHG signal in blue) within an MCA-OVA tumor, 7 days after adoptive transfer in a mouse treated with 100 mg/kg CP. OTI T cell track paths with a straightness of >0.5 are in purple and those with a straightness of <0.5 are in white.
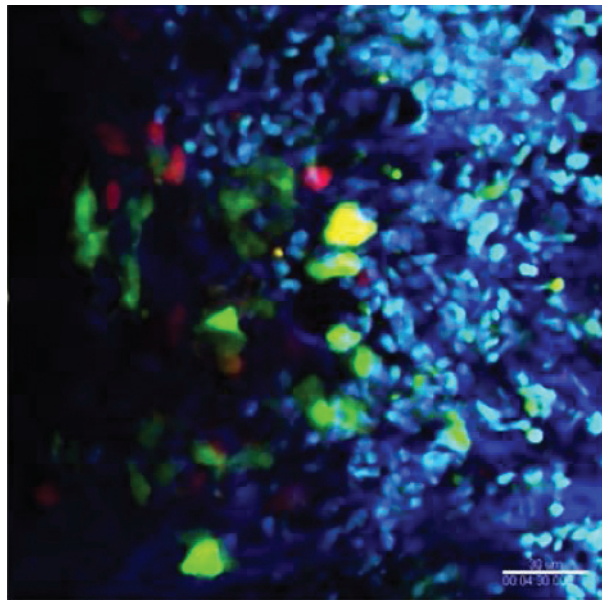
Movie W9. OTI T cell dynamics in different regions of the tumor. Time-lapse TPLSM video showing OTI-DsRed cells (red), CD11c-YFP$^+$ cells (green), DAPI$^+$ dead cells (cyan), and collagen fibers (SHG signal in blue) within an MCA-OVA tumor, 7 days after adoptive transfer in a mouse treated with 100 mg/kg CP.